metals

MDPI

Article

One-Step Enameling and Sintering of Low-Carbon Steels

Miguel Angel Martinez [1], Juana Abenojar [1,2,*], Mohsen Bahrami [1] and Francisco Velasco [1]

[1] Material Science and Engineering Department, Universidad Carlos III de Madrid, Av. Universidad 30, 28911 Leganes, Spain; mamc@ing.uc3m.es (M.A.M.); mbahrami@ing.uc3m.es (M.B.); fvelasco@ing.uc3m.es (F.V.)

[2] Mechanical Engineering Department, ICAI, Universidad Pontificia Comillas, Alberto Aguilera 25, 28015 Madrid, Spain

* Correspondence: abenojar@ing.uc3m.es; Tel.: +34-916249401

Abstract: Powder technology allows manufacturing complex components with small tolerances, saving material without subsequent machining. There is a growing trend in using sintered steel components in the automotive industry. Within 2020, about 2544 million US dollars was invested for manufacturing sintered components. Not only does this industry uses steel components, but the gas cooker industry also uses steel in its burners since they are robust and usually demanded by Americans, with forecasts of 1097 million gas cookers in 2020. Steel gas burners have a ceramic coating on their surface, which means that the burner is manufactured in two stages (casting and enameling). This work aims to manufacture the gas burners by powder metallurgy, enameling and sintering processes in a single step. To achieve this aim, the ASC100.29 iron powder has been characterized (flow rate, relative density and morphology); subsequently, the most suitable parameters for its compaction and an adequate sintering temperature were studied. Single-step sintering and enameling was achieved by compacting iron powder at 500 MPa and sintering at 850 °C for 5 min. The necessary porosity for mechanical anchoring of the coating to the substrate is achieved at this sintering temperature. Bending resistance tests, scratching, degradation under high temperature and basic solution and scanning electron microscopy were used to characterize and validate the obtained samples.

Keywords: powder metallurgy; steel; sintering; enameling

Citation: Martinez, M.A.; Abenojar, J.; Bahrami, M.; Velasco, F. One-Step Enameling and Sintering of Low-Carbon Steels. *Metals* **2021**, *11*, 1007. https://doi.org/10.3390/met11071007

Academic Editor: Pasquale Cavaliere

Received: 23 May 2021
Accepted: 21 June 2021
Published: 24 June 2021

1. Introduction

Enameling is an ancient technique used in the arts (jewelry, badges and brooches) [1]. Enamel is a glassy inorganic powder deposited onto a metal substrate; then, it is melted on it. The molten powder provides a compact coating and gives strength and hardness to the metal and aesthetics. From 1600 BCE, enameling has been developed to decorate objects or protect them against corrosion or the environment. It became popular when it received tremendous interest in improving engineering properties such as wear and chemical resistance [2]. Furthermore, it is essential to distinguish traditional glazes (for ceramic materials) from enamels (glazes on metal substrates). Enamels usually have a low softening point (800–900 °C, depending on the specific powder used), rich in cobalt and titanium, which melt on metals [3].

Silica is the main component of the enamel, but it has a high melting temperature; thus, it needs fluxes, such as borax (sodium tetraborate in its anhydrous form ($Na_2B_4O_7$) and alkaline oxides such as sodium, magnesium, potassium and calcium oxides), to produce borosilicates. On the other hand, in order to improve the resistance to temperature, chemical products, abrasive enamels and refractory materials, such as alumina (Al_2O_3), are used, providing an amorphous appearance [4]. In addition to these components, enamel needs to form a metallurgical bond in the interfacial region with the metal; hence, the presence of Ti, Cu, Cr and Co in enamel compositions can play the role of adhesive agents [5,6]. These

elements also protect the metal surface from chemical attacks (acids, rust, corrosion, etc.) and provide the desired color in conjunction with opacifiers and coloring agents such as titanium dioxide (TiO_2). Furthermore, adhesive agents promote the formation of ferrite spinels on the interface, such as $CuFe_2O_4$ and $CoFe_2O_4$ [7].

There are some well-known applications for enameled materials, such as odontology and kitchenware [4]. This is due to their outstanding resistance to heat, thermal shock and direct flame [8,9]; furthermore, enameling has good resistance to aggressive chemicals and abrasion. Their surface is easy to clean, especially if they contain TiO_2 for photo-catalytic function since it acts as a virus killer [10,11].

Glazes are thin glassy layers (usually 0.15 to 0.5 mm thick) formed on the ceramic body that is subsequently fired at a suitable temperature to flow. The evolution of these finishes makes it possible to differentiate between traditional glazes—that are silicic—and non-traditional, which are mainly made of polycrystalline systems (oxides, carbides, nitrides, silicides, etc.) [12].

The enamel composition will be fundamental in its stability and needs to be optimized so that the working environment does not affect it. If the enamel contains some soluble components in ambient humidity, they can produce a network of fine cracks; they can lose gloss or hue or even cause a loss of adhesion that would lead to flaking. Consequently, substrate corrosion can occur on the metallic component. These soluble components are alkaline oxides, which are used as fluxes. However, this can be modified with the addition of alumina and zirconia, or barium and calcium, which can form insoluble silicates [8]. Although enamel presents corrosion protection and high hardness, its resistance to abrasive wear can be compromised due to the low fracture toughness. Abrasive wear will depend on the chemical composition of the frit. Rossi et al. [13] tried to improve abrasive wear resistance by adding hard particles such as quartz, WC or SiC. Quartz particle fillers improved the abrasion resistance of frit, whereas filler with SiC and WC particles modified the wear mechanism of the coating. This wear improvement was due to the excellent interface between the enamel matrix and particles that reduced the crack nucleation.

Nowadays, anticorrosive coatings play an essential role in protection methods due to their versatility and acceptable costs [14]. Paints or polymeric, metallic and ceramic coatings can be applied as a protection layer. Many industrial paints are used currently; however, they have neither a good chemical resistance [15] nor temperature resistance. However, paints or polymer coatings can be improved by adding fillers such as silica to increase wear resistance [16], or Nb_2O_5 to improve chemical resistance in the acid medium [17], etc. The ceramic powders can also be used as a coating on metallic components once they are sintered. This coating protects the metal from corrosion or oxidation, improving wear resistance and mechanical properties. For example, ceramics such as yttria-stabilized zirconia are used as a thermal barrier coating on Incone 738 superalloy [18]; they reduce the thermal oxidation and corrosion rate. Other applications with titanium or magnesium can make them compatible with implants. Specifically, in magnesium alloys that are very easily corroded, a coating with modified hydroxyapatite produces a biometric layer that improves corrosion resistance and biocompatibility [19].

The most common techniques to deposit ceramic protection coatings have been known for a long time: sol-gel processing, physical or chemical vapor deposition, evaporation, sputtering, laser-induced deposition, ion implantation, and electrolytic deposition [20,21] are some important examples. Another advanced common technique to make coatings is a thermal spray. It is widely used in industrial applications, such as aerospace, automotive, chemical and petrochemical industries. Among the thermal spray techniques, the flame spray method is the most used one; it is a simple and economical technology that protects the substrate against corrosion and provides good mechanical properties [22]. In addition, since flame spray coatings are carried out with metallic alloys [23], they have good resistance to high temperatures [24].

On the other hand, powder metallurgy (PM) is another production process based on the compaction and sintering of metal powders to produce high-quality parts with complex

shapes, very tight tolerances, and relatively inexpensive ways [25]. This technology has been utilized for ages, and nowadays, many researchers continue to work on this concept looking for new applications, keeping in mind their advantages and limitations [26].

PM manufactured samples can be coated to improve hardness; Franco et al. [27] created M2 high-speed steel hardened by niobium carbides or niobium borides and iron borides. Moreover, they also achieved a good wear resistance by the borinizing process.

PM is a technology applied to many metals, such as steel [28–31], stainless steel [32–34], aluminium [35,36], copper [37], titanium [38–41], and magnesium [42,43], etc. Metal powders can be pre-alloyed [44,45] or mechanically alloyed [34,46]; it depends on the application sought. PM seeks added value for use on an industrial scale, such as biomedical implants using wear-resistant titanium alloys [47–49] or in the manufacture of hard metals for cutting tools or coatings [50]. Currently, one of its main applications is in the automotive industry for the manufacturing of small and complex components. The parts manufactured from iron powders in the automotive industry in 2020 are estimated at 2544 (millions of US dollars) [51]. The manufacturing of metal matrix composites (MMC) also employs PM [52], wherein the reinforcement phase could be ceramics, such as cemented carbide or cermet [53,54]. MMC materials can improve corrosion, wear and high-temperature resistance in addition to mechanical properties.

On the one hand, PM technology provides components with open porosity, which are easily damaged by external agents and can suffer corrosion, not just superficially but also internally. On the other hand, the surface porosity provides the roughness necessary for mechanical bonding of the enamel [55], in addition to the chemical bonding related to the adhesion agents it contains. Industrial steel components coated with this enamel are manufactured in two steps: casting and grinding of parts, followed by electrophoretic or sprayed coating and heating. This work aims to sinter steel components and coat them with a ceramic enamel powder within a single step at a low temperature, thus saving energy and time. Enamel temperature (850–900 °C) is low for steels, which are usually sintered above 1120 °C [56]. The low softening point of enamel is a requirement to avoid damaging the structure of the metal support.

According to the EN 10209: 2013 standard [57], the enamelable steels and irons are cold-rolled ones; thus, they are low carbon steels with ferrite or ferrite with some pearlite; harder structures by deformation. In addition, based on the EN 10025-2: 2020 [58] and EN 10111: 2009 standards [59], they can be hot-rolled steels such as unalloyed ones for low carbon steels.

With this aim, low carbon ASC 100.29 iron powder is used, which is characterized before and after sintering. The main uses of these parts are gas burners in kitchens (Figure 1). The household cooking market revenue forecast in 2025 is USD 124.8 billion [60], in which emerging countries such as China, India or Brazil will be the proper drivers of this growth. The gas cooktop accounts for around 38% of the total household cooking.

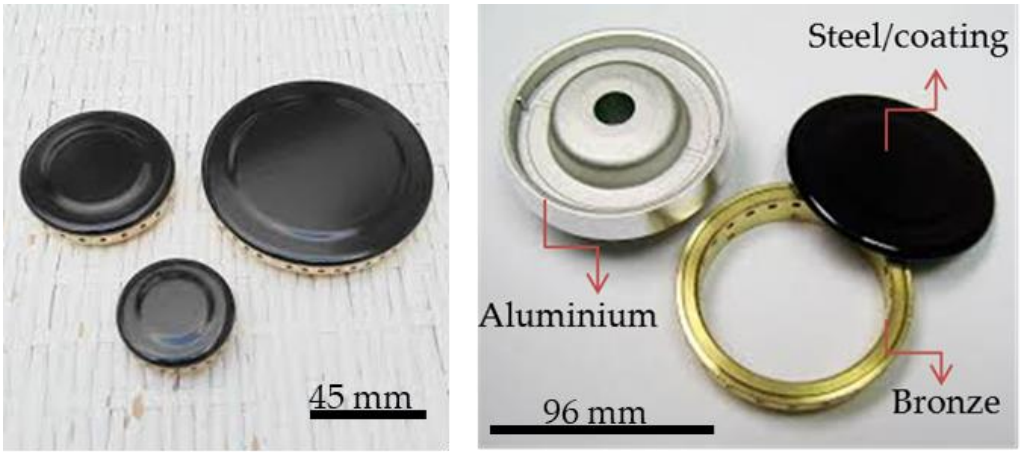

Figure 1. Burner caps from Teka (Spain) [61].

2. Materials and Methods

2.1. Materials

The used iron powder was ASC 100.29 from Höganäs AB (Höganäs, Sweden). It is water atomized powder with very high purity (+99.9% Fe, <0.01% C, 0.08% O) and compressibility, making it possible to reach the density of 7.2 g/cm^3 with a single pressing. It is particularly suitable for high-density structural parts and base material for magnetic applications [62,63].

For coating, MS3325 porcelain enamel powder supplied by Ferro Spain S.A. (Almazora, Spain) was used. It is a greasy powder with a grey color composed of frit (alkali borosilicate) and a binder. It has good resistance to acids and alkalis, pyrolytic performance, high hue and gloss level. It is formulated for electrostatic application in dry form, although it can be applied by spray or paintbrush with the appropriate diluent. Furthermore, it can be applied on decarburized iron with a recommended working temperature of 820 °C [64].

2.2. Powder Characterization and Green Properties

The characterization of the iron powder was carried out by measurement of the apparent density according to the EN ISO 3923-1: 2011 standard and the flow rate measurement with a Hall flowmeter or funnel calibrated based on the EN ISO 3923-1: 2011 standard. In addition, particle size distribution was also measured by a Mastersizer 2000 (Malvern, UK).

The iron powder was compacted in a uniaxial press (Microtest, Madrid, Spain) at different compaction pressures from 300 to 700 MPa. The dimensional variation and density of the obtained materials were studied in this stage according to the EN 3927: 2002 standard. The dimensional variation was made by the difference between the dimensions of green samples and the compacting die (31.40 mm × 12.60 mm). This elastic expansion is known as spring-back. Moreover, the die walls were lubricated with zinc stearate (lubricated die).

The mechanical properties of green components were studied by the three points flexural test according to the EN ISO 3325: 1996 standard. The load cell was 150 N, and the test was carried out at a speed of 1 mm/min in a universal testing machine by Microtest (Madrid, Spain).

2.3. Sintering Properties

The properties of sintered components concerning their associated costs give an idea of the efficiency of the sintering process. Temperature and time are the most critical parameters to control the sintering process. A stainless-steel furnace with a temperature controller from 400 to 1250 °C was chosen for sintering, supplied by Microtest (Madrid, Spain). The sintering atmosphere was N_2-5H_2. Into the oven, there is overpressure since the gas was bubbled on water constantly. The sintering cycle was heating at 5 °C/min from room temperature to the chosen temperature, which was kept for 30 min, then cooling at 20 °C/min until 100 °C, to open the furnace.

Sintering was carried out at six different temperatures, 1080 °C, 1030 °C, and lower temperatures from 800 to 900 °C, that allow sintering and enameling in a single step. It is worth mentioning that enamel needs porosity to achieve reliable anchoring with the steel. Thus, high sintering temperatures, which result in full dense enamel, cannot be applied. In this regard, two higher temperatures were used to study the densification behavior and compaction pressures. The four lower temperatures were used to balance the mechanical properties and enameling parameters such as time.

In this regard, 125 specimens with a dimension of 31.5 mm × 13 mm were manufactured. With these specimens, the density, dimensional variation, mechanical resistance to bending, and elemental chemical analysis of carbon, oxygen and nitrogen were investigated (LECO TC 500 and CS 200, Leco Instrument, S.L. Madrid, Spain).

In addition, two specimens with the same dimensions were manufactured per condition to study which factors have the most significant influence on enameling and material characteristics.

The powder morphology and topography of sintered samples were analyzed by scanning electron microscopy (SEM) (Jeol JSM-840 SEM, Tokyo, Japan), which allows providing elemental identification and quantitative compositional information by energy dispersive X-ray analysis spectra (EDX or EDS). In this regard, enamel powder was also characterized by SEM and EDS. Furthermore, X-ray fluorescence (SPECTRO XEPOS III, Ametek, New Bedford, CA, USA) was also used for the chemical analysis of enamel.

2.4. Enameling

The most crucial thing in this section was achieving fluid enamel that is easy to apply, which will not leave lumps and is evenly distributed. In the enameling process, the amount of water or dispersants needs to be optimized to facilitate the application of enamel. Disperbyk 199 and Disperbyk 154 by B.Y.K. Additives and Instruments (Wesel, Germany) were used as dispersants. Both have water solvents and should be added before enamel. Other possibilities are using the dispersants in water with 0.1 wt% NaOH (caustic soda—sodium hydroxide) or only water.

2.5. Characterization of Coating Adhesion

Two different tests were carried out on coated samples entirely to check the coating adhesion. One of them was at a high-temperature, and another was in a basic medium. A high-temperature test was performed with a flame at 900 °C with alternate heating and cooling cycles up to room temperature 100 times. An immersion test was done in a NaOH solution of 0.5 M for one month.

Results were evaluated after each test by digital microscopic Olympus DSX1000 (Olympus, Barcelona, Spain) with a DSC10-XLOB lens. The main sought-after defects were polishing, cracking, spoiling, and apparent change in the coating color. In addition, the coating was tested according to the ISO 1518:2011 standard, in which a fixed load is used on a hemispheric needle to scratch the surface (Figure 2). This test was carried out with a Clemen Scratch tester by Neurtek Instruments (Eibar, Guipúzcoa, Spain). This test is much more aggressive than a wear test since there is 4 kg on a metal punch, so the load is not distributed. The resulting trace is analyzed to determine the delamination of coating on the substrate. Tests were conducted on a "go/no go" basis using a single specified load from 2 to 4 kg.

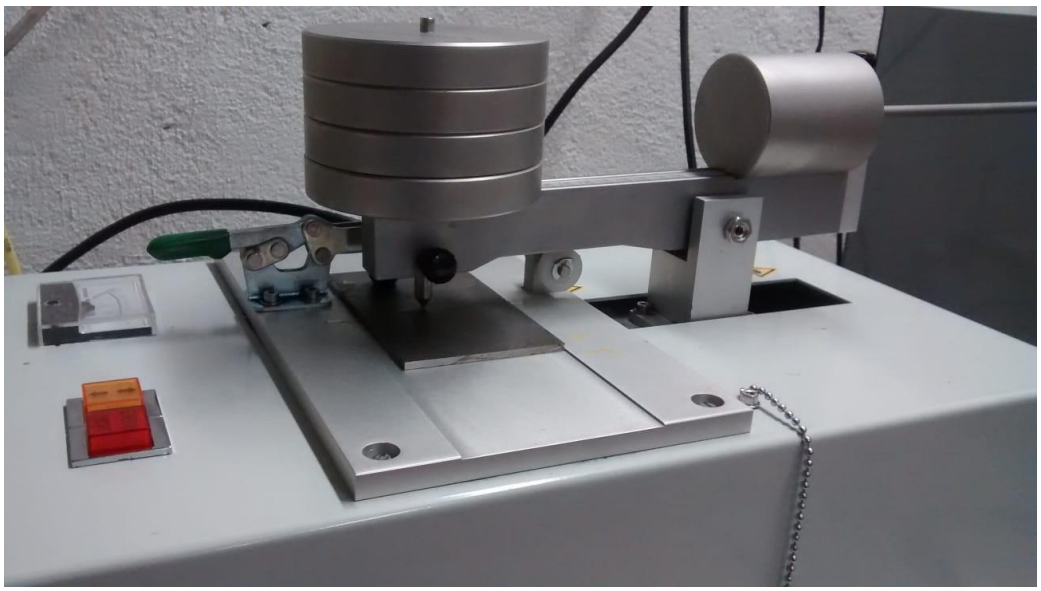

Figure 2. Clemen Scratch tester with a 4 kg load.

3. Results

3.1. Powder Morphology and Properties

According to Figure 3A,B, iron powder ASC 100.29 is irregularly shaped as it is a powder atomized in water. It has an apparent density of 3.02 g/cm^3 and a flow rate of 26.52 s/50 g (Table 1), allowing easier cavity die filling. The average particle size is 97 µm. According to Figure 4, the size distribution for d (0.1), d (0.5) and d (0.9) is 43, 97 and 193 µm, respectively; being d (0.1), d (0.5) and d (0.9) the 10%, 50% and 90% of the volume distribution below the indicated value. This distribution allows the powder to be repositioned, leaving few gaps between the particles, so the density after compaction will be high.

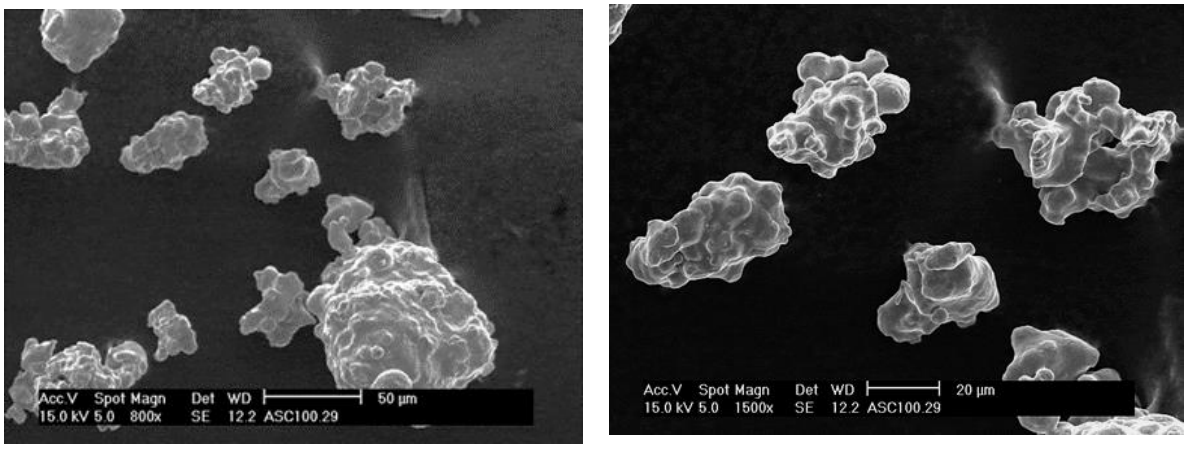

(**A**) (**B**)

Figure 3. Micrographs of iron powder ASC100.29. (**A**) Magnification 800× and (**B**) Magnification 1500×.

Table 1. Apparent density and flow rate of iron powder ASC100.29.

Iron Powder	Apparent Density (g/cm^3)	Flow Rate (s/50 g)
ASC100.29	3.024 ± 0.004	26.52 ± 0.25

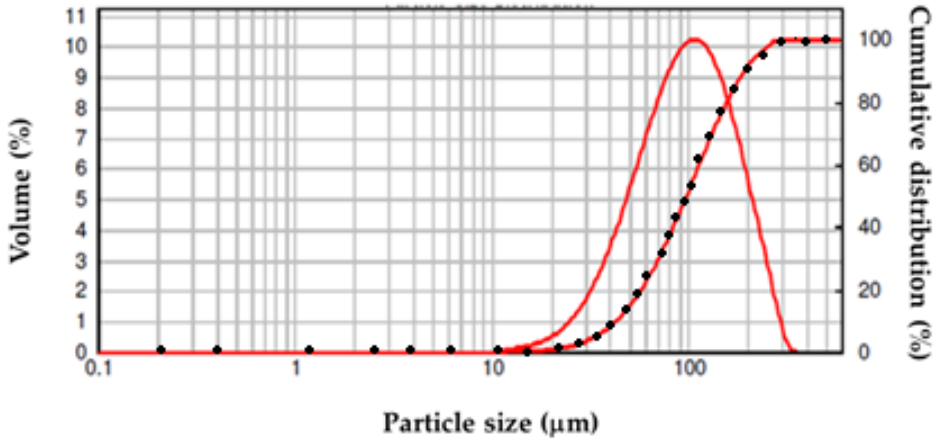

Figure 4. Particle size distribution of ASC100.29 iron powder (red line corresponds to volume (%), and the dotted line is cumulative distribution (%)).

The powder morphology of MS3325 enamel powder can be seen in Figure 5A. There are larger particles around 25 µm, mainly with polygonal form and pronounced edges. In addition, Figure 5B shows smaller white particles, which can correspond to fluxes (Figure 5A) or other components added to the frit. Distinguishing the other particles with

a more amorphous shape is difficult since some cover the other; they are small particles with a foam appearance. EDS made it possible to know these components through analysis at different points of the micrograph shown in Figure 5B. In this regard, larger particles correspond to the silica, and smaller ones (point 5) correspond to the alumina, and other white particles with a polygonal form are chromium oxide (point 4). Figure 5C shows the spectrum of spot 1, and Table 2 summarizes all analyses.

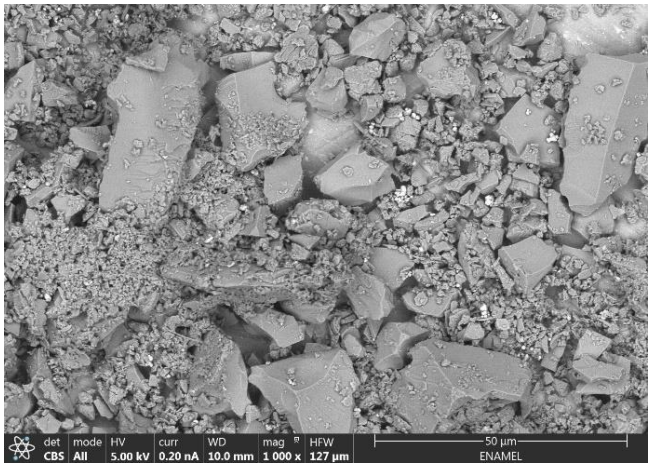

(**A**)

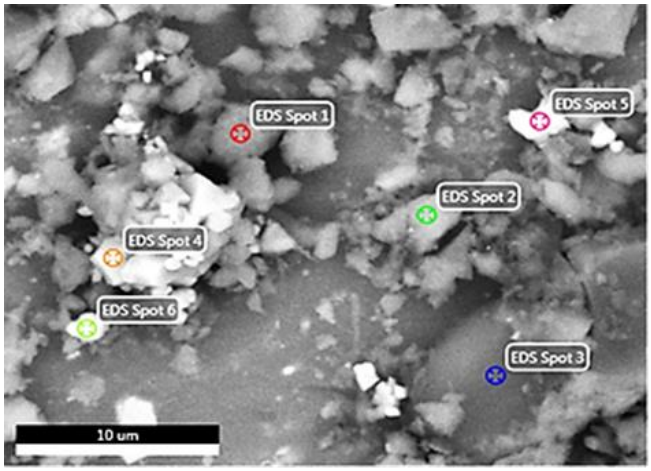

(**B**)

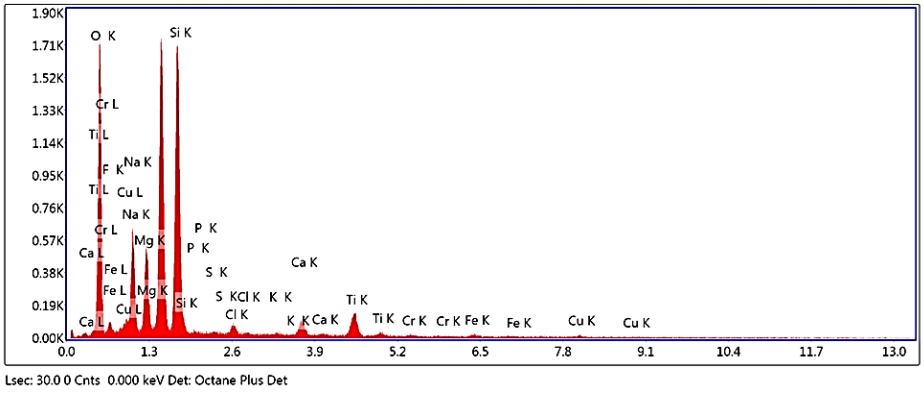

(**C**)

Figure 5. (**A**) SEM micrograph of enamel powder, (**B**) micrograph of EDS study, and (**C**) EDS on spot 1 of Figure 5B.

Table 2. Chemical analysis of frit in different points of Figure 5B.

Elements	Spot 1	Spot 2	Spot 3	Spot 4	Spot 5	Spot 6
	Weight%					
O K	47.98	50.72	35.18	8.59	35.48	29.65
Si K	19.13	17.15	36.72	1.54	3.77	2.85
Na K	13.05	11.86	5.22	-	4.41	4.95
K K	0.09	-	2.08	-	-	-
Mg K	7.93	7.41	1.41	-	1.27	1.29
Ca K	1.6	1.39	8.58	1.33	0.36	0.34
Al K	-	-	-	-	10.89	-
Mn K	-	-	-	7.33	2.97	5.87
Ti K	3.18	2.91	5.33	-	-	-
Cr K	0.16	-	-	18.36	14.05	14.44
Fe K	0.49	0.34	-	28.51	9.02	17.79
Cu K	0.21	0.52	1.04	2.25	-	1.11
Co K	-	-	1.84	20.4	11.24	17.5
Ni K	-	-	3.23	9.91	2.76	3.67

Chemical analysis (Table 2) shows the presence of silicon, sodium, potassium, magnesium, calcium, aluminum, titanium, manganese, iron, chromium, cobalt, nickel, and copper, with oxygen as main elements, in addition to fluorine (4 wt %), carbon (2 wt %), chlorine (0.5 wt %), and sulfur (0.2 wt %) in some spots, which can also be contra ions.

It is consistent with what has explained in the introduction that the components of the frit are mainly silica with additives such as alumina (refractory material), flux and metals (Ti, Mn, Cr, Co, Ni and Fe as adhesive agents) to provide chemical anchoring in the interphase between enamel and steel.

X-ray fluorescence analysis also gave information on present oxides in the frit. This technique makes it possible to have a total vision of the composition since EDX is punctual and qualitative but never quantitative. In this regard, silica is the majority element with 60 wt %, fluxes in total are 27 wt % (Na_2O and MgO with 16 and 7 wt %, respectively, the most abundant). Refractory material (Al_2O_3) is present at 5 wt %; the rest are the adhesive agents present at 8 wt %. The three most important adhesive agents are TiO_2, NiO and CoO with 3.5, 1.8 and 0.9 wt %, respectively; MnO, FeO, and CuO are in less proportion.

3.2. Compressibility Curves and Green Properties

ASC 100.29 iron powder was compacted at different pressures, from 400 to 700 MPa. As expected, the density increased with increasing the compaction pressure to a maximum at 700 MPa (Figure 6A). The density is affected by the stress created within the powders by the pressure. The green sample is expanded after removing the die to reduce this internal stress (Figure 6B). This expansion in the longitudinal direction is less than 0.25% and lower than 0.5% in the width direction. In addition, the green bending strength also increases with the compaction pressure (Figure 6C); it achieves 55 at 700 MPa. This value is very high compared to 38 MPa of Höganäs [59] for compaction pressure of 600 MPa. Both cases were done with a lubricated die. Relative density provides an idea of the porosity of the samples (Figure 6D). It is evident that low compaction pressures have a lower relative density and therefore higher porosity, thus at 500 MPa, the samples present 12% porosity; however, at 400 MPa, 17%.

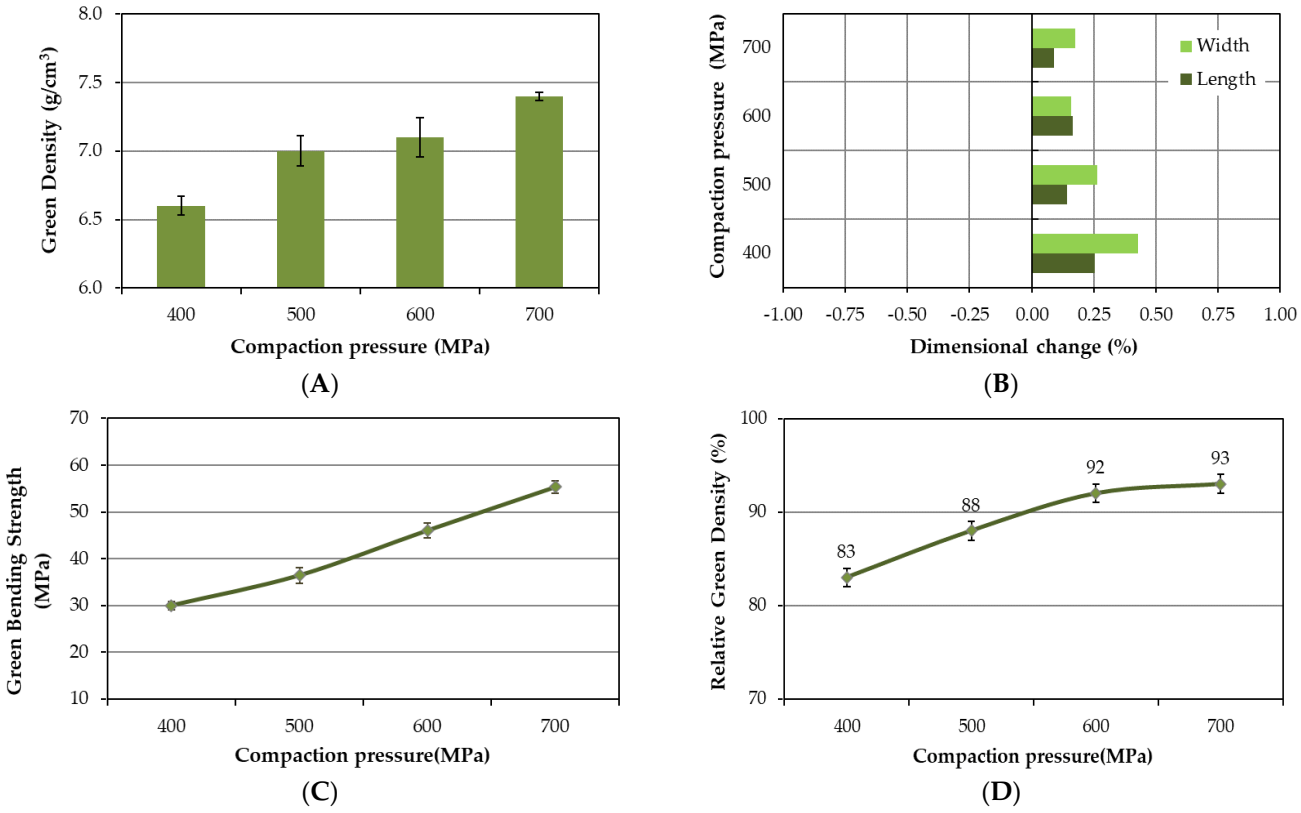

Figure 6. Variation of green properties with compaction pressure: (**A**) density, (**B**) dimensional variation, (**C**) bending strength, and (**D**) relative green density.

3.3. Properties of Sintered Specimens

The densification behavior is shown in Figure 7. As expected, the density decreased with the temperature and pressure of compaction. Figure 7A indicates that the decrease in compaction pressure seems more important than the temperature. For example, at 700 MPa, the density changes from 7.63 to 7.34 g/cm^3 when temperature decreases from 1080 to 820 °C. However, for 1080 °C, the density changes from 7.63 to 6.89 g/cm^3 if compaction decreases. Figure 7B exhibits the relative density, which is related to the porosity of samples. The compaction pressures at 700 and 600 MPa show relative density over 90%; thus, the porosity is less than 10%, independent of sintering temperature.

On the other hand, in the densification, both compaction pressure and sintering temperature play the same role (Figure 7C). In general, densification is more significant for high compaction pressure and high sintering temperature than low pressures and temperatures. For example, at 500 MPa, the effect of sintering temperature is weak.

By considering the longitudinal dimension variation (Figure 7D), contractions are constantly observed, although they are small and not very important since they are below 0.5%. This value is accepted in PM because it is less than the permitted tolerance.

As a result of the sinterability study, low sintering temperatures (835 or 820 °C) together with high compacting pressures (700 or 600 MPa) may work well for subsequent enameling.

Low-temperature sintered specimens were prepared to calculate the bending strength and elongation, as shown in Figure 8.

These data (Figure 8) help to choose the appropriate compaction pressure and sintering temperature. The sintering temperature of 820 °C is too low for enameling (as it will be seen later). Moreover, high compacting pressure (700 MPa) provides porosity around 14% (Figure 7C) at 835 °C. Nevertheless, at 500 MPa, porosity drops a bit, 10% at 835 °C and up to 5% at 820 °C. Accordingly, 500 MPa is chosen as the compaction pressure. On the other

hand, bending strength and elongation need to be considered. If 500 MPa is applied, the sintering temperature may be increased to improve the mechanical properties.

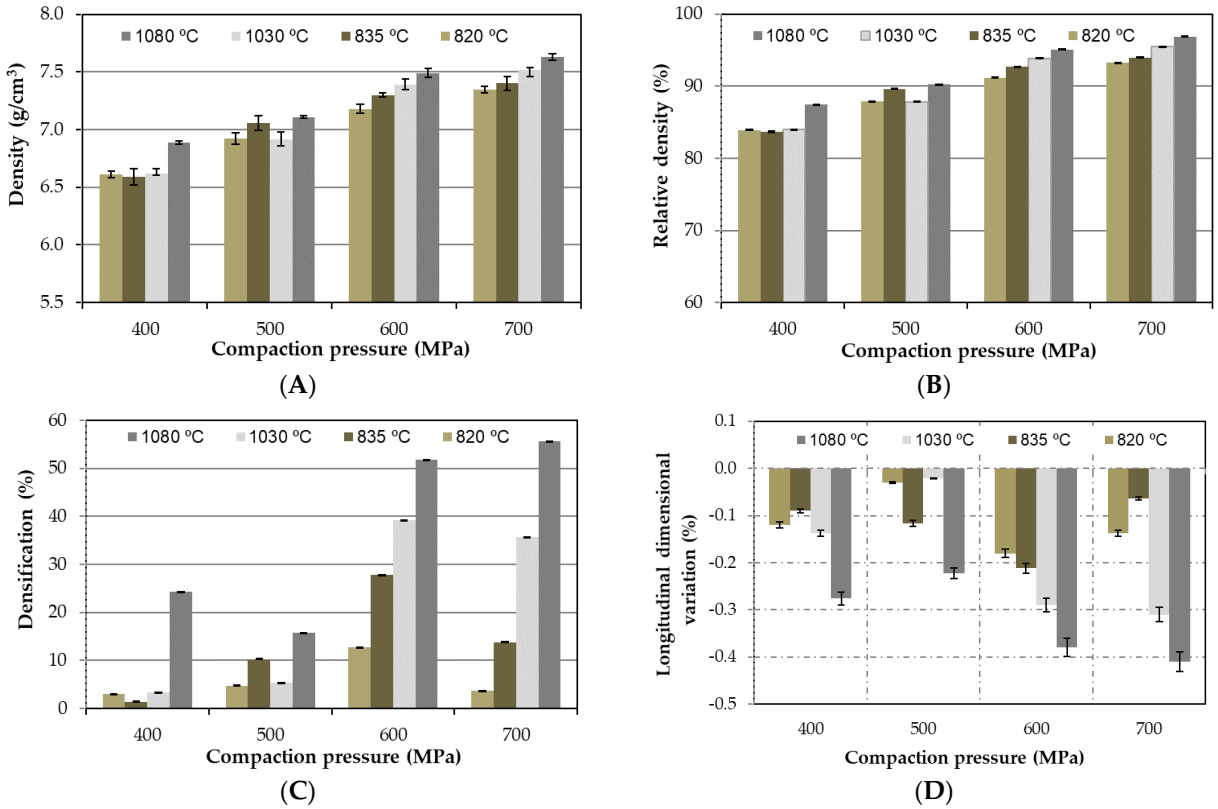

Figure 7. Densification behavior of ASC 100.29 (**A**) density, (**B**) relative density, (**C**) densification, and (**D**) longitudinal dimensional, versus compaction pressure at different temperatures.

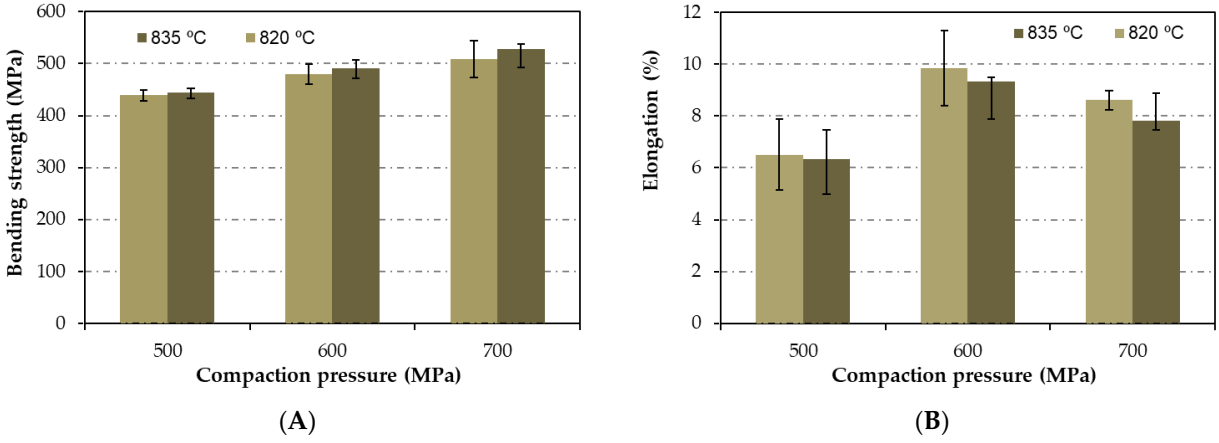

Figure 8. (**A**) Bending strength and (**B**) elongation at low temperatures sintering versus compaction pressure.

Once the bending strength of samples was tested, the fracture surfaces were observed by SEM (Figure 9). Ductile fractures are evident in the micrographs due to dimple formation. The cohesion between the grains is higher (Figure 9A–C) when the sintering temperature is 835 °C compared to Figure 9D sintered at 820 °C. Nevertheless, there is practically no difference among Figure 9A–C, so the compaction pressure at this temperature has very little influence.

To control possible problems with a sintered atmosphere, the percentages of carbon, oxygen and nitrogen were analyzed in the samples compacted at 500 MPa and sintered at

835 °C (Figure 10). The oxygen content is minimal, with the highest quantity of 0.1%, equivalent to the powder's oxygen. The amount of carbon is even lower, between 2.5×10^{-3} and 6×10^{-3}%, within the equipment's error percentage (<0.01%). Since the amount of nitrogen is low as well, the sintering atmosphere has not affected the powder composition. Therefore, it can be said that there is no oxidation during sintering, and it is ferritic steel.

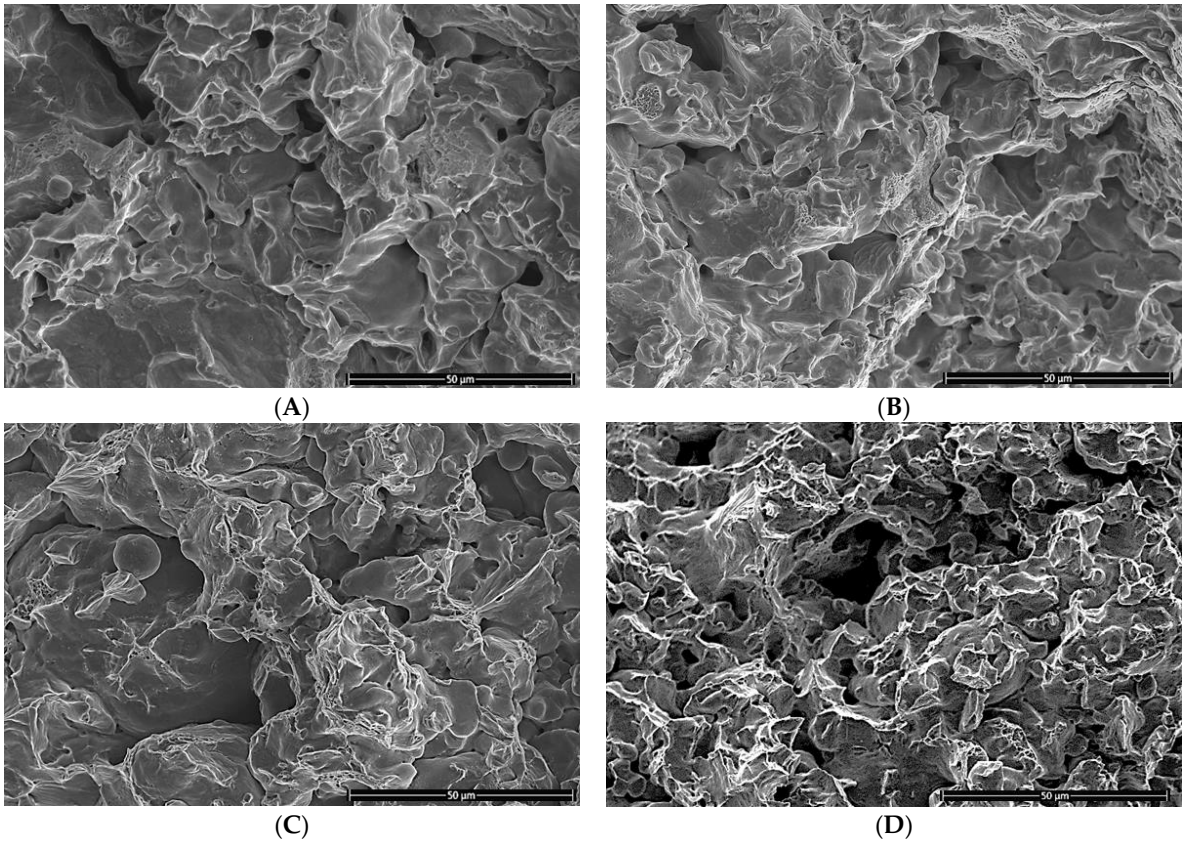

Figure 9. Fracture micrographics by SEM of sintered samples at (**A**) 835 °C at 700 MPa, (**B**) 835 °C at 600 MPa, (**C**) 835 °C at 700 MPa and (**D**) 820 °C at 500 MPa (magnification bars are 50 µm).

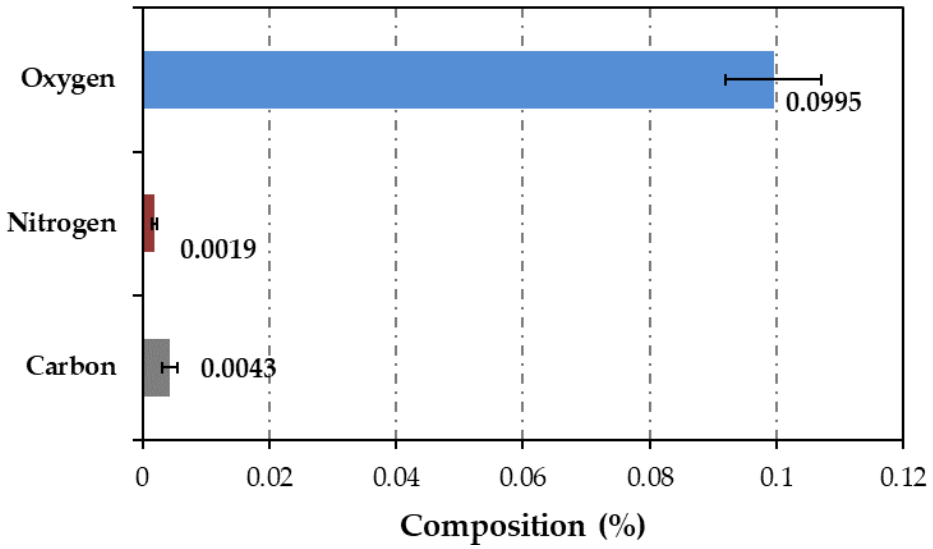

Figure 10. Chemical analysis of carbon, nitrogen and oxygen carried out by LECO for samples compacted and sintered at 500 MPa and 835 °C.

3.4. Enameling Properties

The dispersants and NaOH solution resulted in shrinkage and rust of the enamel. Thus, after many tests, the best condition was water as the solvent, high viscosity for application with a spatula (around 8000 mPas at 22 °C) and thickness around 100 µm. First, samples at 500 MPa were compacted, then were sintered at 835 °C for 30 min (Figure 11A). The final appearance of the specimens is lumpy. This effect might be because the enamel was thick, and it does not disperse nicely in the water, or because the water evaporates inside the oven all at once. An attempt was made to apply the enamel in a thin layer less viscous, and the processing time was reduced to 5 min. It is also necessary to stop the heating process for one minute at 100 °C to evaporate the water more slowly. As a result, the enameling sample (Figure 11B) has a better appearance than Figure 11A. However, at this temperature, the bending strength is lower than the sample sintered without enamel, around 12%. This is the reason for employing two new temperatures of 850 and 900 °C for enameling and sintering in a single step.

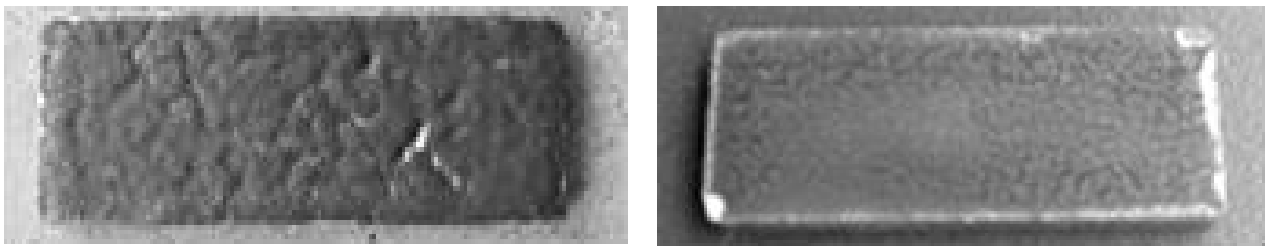

(**A**) (**B**)

Figure 11. Macrographics of sintered and enameled samples in one step at 835 °C and different times: (**A**) 30 min and (**B**) 5 min.

Figure 12 shows the bending strengths and elongations for different temperatures and times. The samples sintered and enameled at 850 and 900 °C for five minutes improved 8% and 9% in terms of the bending strength and 57% and 66% for elongation, with respect to sample sintered at 835 °C.

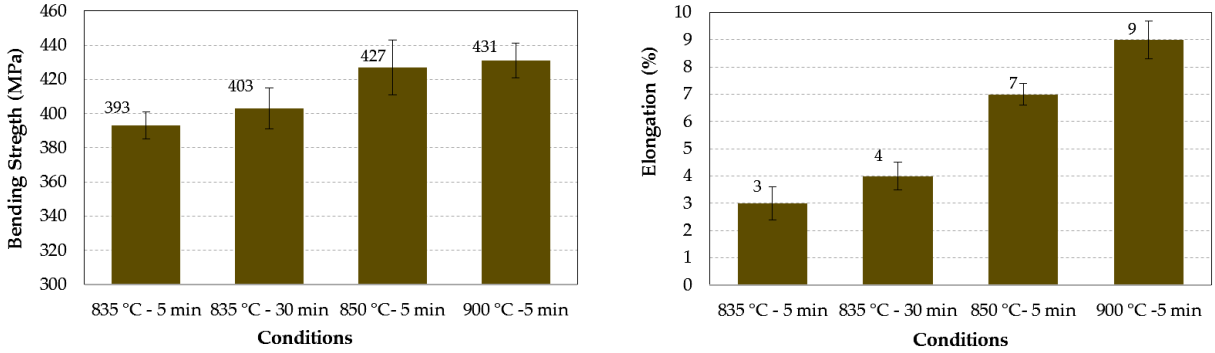

(**A**) (**B**)

Figure 12. Samples sintered and enameled in one step at different temperatures and times: (**A**) bending strength and (**B**) elongation (compaction pressure 500 MPa).

Optical micrographs (Figure 13) show the microstructure of used steel. It is ferritic steel that bonded to the enamel. In Figure 13A, the grains of steel are observed together with the porosity. Furthermore, the enamel is introduced by open porosity and surface irregularities, which resulted in an excellent mechanical anchoring of the enamel. In Figure 13B, bonding details are shown, including the adhesive agents such as chromium, cobalt, nickel, and copper forming compounds on the surface, providing a chemical anchor.

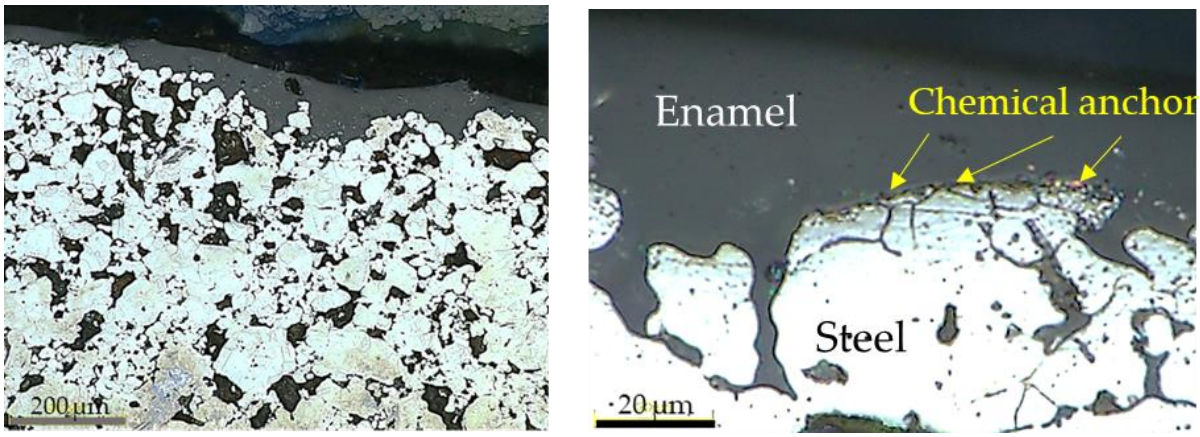

(**A**) (**B**)

Figure 13. Optical micrographs of sample sintered and enameled in one step at 835 °C: (**A**) general overview, (**B**) detail of edge with the enamel after surface attack with 3 v/v% nital (mixture of nitric acid and ethanol).

SEM micrographs of Figure 14 were also taken to observe the influence of temperature on the coating with enamel. Figure 14A,B corresponds to sintering at 835 and 850 °C, respectively, and they show a proper joining between steel and enamel with a mechanical anchor and penetration of enamel into open surface porosity. This effect can be seen more precisely in Figure 14C due to the different compositions that resulted in different grey shades. Furthermore, at 900 °C (Figure 14D), the adhesion is weak; a crack between the steel and the enamel is seen, along with a cracking of the enamel layer.

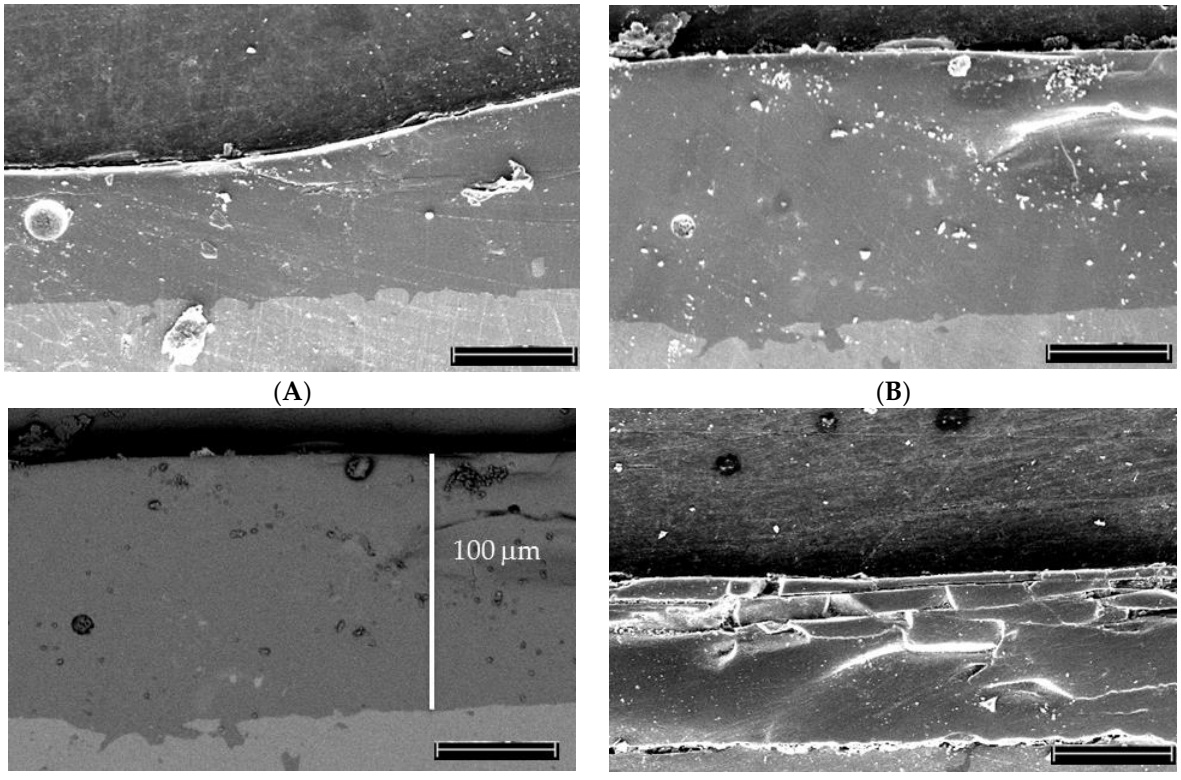

(**A**) (**B**)

(**C**) (**D**)

Figure 14. Micrographics of samples sintered and enameled in one step at different temperatures (**A**) 835, (**B**) 850, (**C**) 850 (in BSE—backscattered electrons) and (**D**) 900 °C (magnification bars are 50 µm).

3.5. Characterization of Coating Adhesion

As-received samples are shown in Figure 15A. It has the same appearance as the samples after fire exposure and immersed samples in NaOH solution (Figure 15B,C, respectively). Their color and gloss did not experience any change. The immersed samples also did not gain weight during the test. After the scratch test, 2 kg load did not produce any damage to the enamels. However, the 3 kg load made a shallow mark by lifting the enamel slightly (Figure 15D). The scratch with the 4 kg load was more profound and more continuous (Figure 15E), but the enamel did not detach, indicating excellent enamel adhesion.

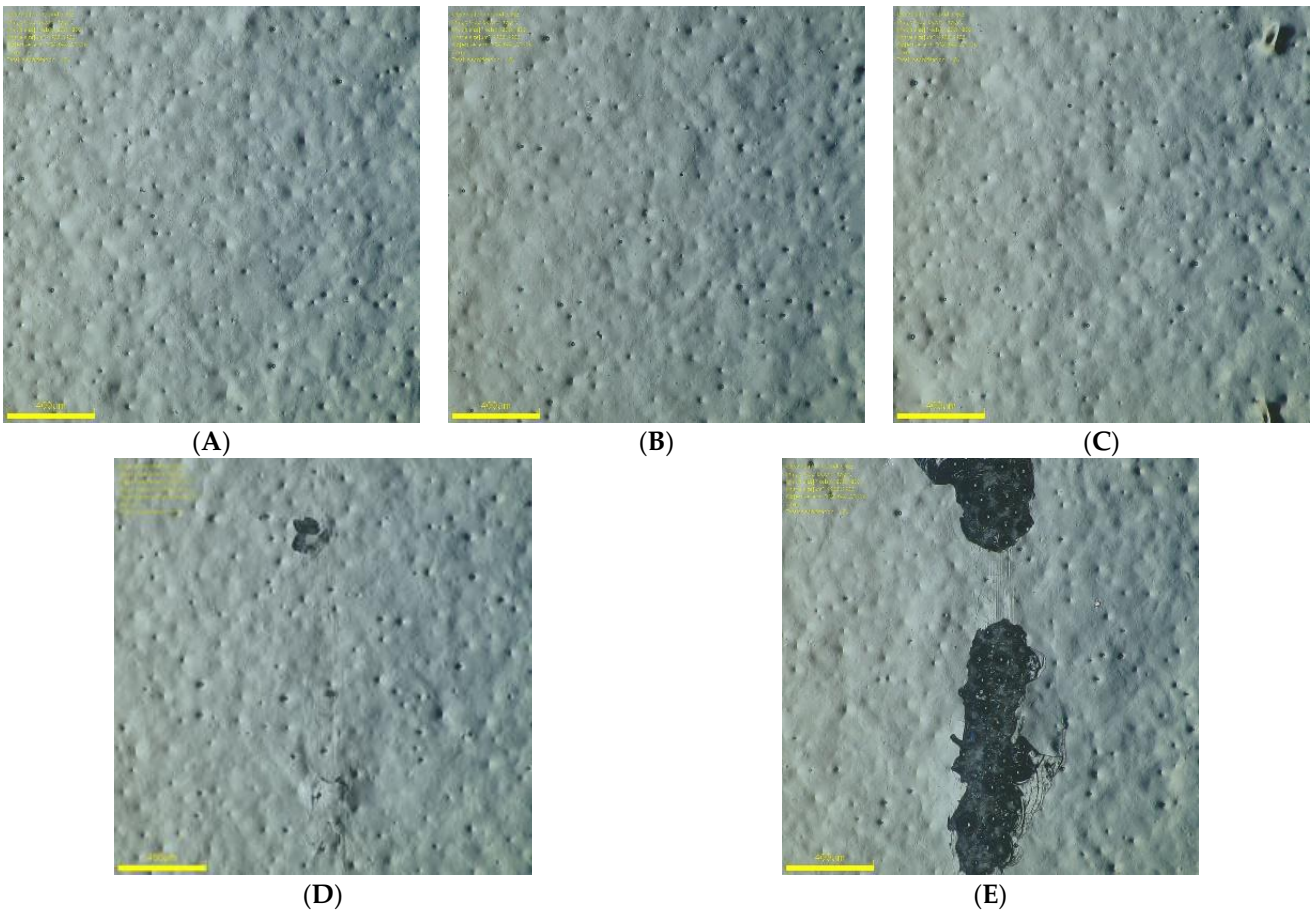

Figure 15. Surface analysis of coated samples: (**A**) without testing, (**B**) after the fire, (**C**) after NaOH immersion, (**D**) tested with 3 kg and (**E**) tested with 4 kg (magnification yellow bars are 400 μm).

4. Discussion

The iron powder chosen for this study provided easy compaction and good sinterability since its shape and distribution size is adequate (Figures 2 and 3). In addition, it has a low carbon content that can facilitate bonding with enamel.

The challenge of this study is to enamel non-laminated powder metallurgical steels, taking advantage of their low carbon content and porosity.

The green samples exhibited lower density for the compaction pressures of 400 and 500 MPa (Figure 6A,D). The pressure of 500 MPa was chosen for this study since it did not show significant differences in density, densification behavior and dimensional variation with higher pressures once the samples were sintered at low temperatures (Figure 7). This effect is due to the tensions created between the powder grains during compaction at high pressures of 700 and 600 MPa, which are then released during sintering.

Regarding the sintering temperature, initially, temperatures close to the one recommended by the supplier of 1150 °C were chosen, although always lower, in this case, 1080 and 1030 °C. The study at these temperatures reported data quite close to those found in the literature; however, these temperatures are high to achieve the main aim of sintering and enameling in a single step. This makes it necessary to sinter first at those temperatures that provide around 12% porosity if the compaction is at 500 MPa (Figure 7B), with subsequent enameling at temperatures between 820 and 900 °C depending on the enamel. Consequently, the two lowest temperatures were studied since the porosity of the pieces at 835 and 820 °C was not significantly different from the highest.

The bending strength (Figure 8A) decreases by 17% at these low temperatures with compacting pressure of 700 MPa at 835 °C to 500 MPa at 820 °C. In addition, according to Figure 9, micrographs at 835 °C are more favorable than 820 °C in terms of more necking zones between iron grains and less breaking. Although elongation at 500 MPa is 6% for both temperatures (Figure 8), it is adequate since after enameling, elongation declines due to the brittle enamel. Consequently, the study was performed on sintered and enameled samples at 500 MPa and 835 °C for 30 min as a reference.

On the other hand, the sintering atmosphere N_2-5H_2 can be maintained, since according to the elemental analysis of C, O and N (Figure 10), neither nitriding nor oxidation of the steel has occurred, and the carbon content has not increased. Nevertheless, all of them may be dangerous for enamel adhesion.

The enamel was characterized to know its components. This type of enamel contains adhesive agents such as cobalt, chromium, nickel, copper, and iron in the form of oxides (Table 2 and Figure 5C) to react with the iron on the samples' surface to obtain a chemical bond [4,8]. Furthermore, the enamel application had to be optimized, so it was necessary to do tests with dispersants, diluted caustic soda and water. The utilized dispersants did not work as the enamel lost adherence (Figure 2) or rapidly oxidized the sample's surface. In some cases, the enamel itself rusts, for example, with caustic soda. The best results were obtained with water as a dispersant, and it was applied by spatula in the ratio of 0.2, which means 100 g of enamel in 20 mL of water.

During the enameling process, different stages take place. First, the water needs to evaporate. To prevent rapid evaporation, the heating stops around 100 °C for 1 min, at about 500 °C, enamel degassing also occurs, and iron oxidation begins. At the same time, possible organic contaminants on the surface of the sample are removed. In the third stage, the temperature of which depends on the added fluxes (borax and sodium, calcium, magnesium and potassium oxides (Table 2)), the enamel softens and begins to wet the steel; in this case, it occurred around 750 °C. At the same time, during the sintering process, there is diffusion between enamel and substrate. They create a transient layer with the Fe of substrate and Co and other adhesion agents. According to Bodaghi and Davarpanah [5], adhesive agents significantly improved the adherence index and reduced spraying time. In addition, the effectiveness of bonding agents to promote bonding is associated with a galvanic attack. Then at 750 to 860 °C, there is saturation at the interface of iron oxides and the possibility of oxygen anions penetration in the enamel that would create bubbles in it. In the case of steel, spinels are formed on the interface. These spinels are typically formed at 1000 °C [65,66], but the presence of fluxes can reduce this temperature. Those spinels form in the interface, and the roughness of the substrate provided good enamel adhesion, as shown in Figures 13 and 14. Therefore, there are three adhesion mechanisms: mechanical, chemical and diffusion, since during the enameling process, the adhesion agents diffuse across enamel and form spinels at the interface of steel and enamel.

The bending strength was studied in Figure 12. Two new temperatures were tested to achieve high bending strength and good enameling. According to the results, the chosen temperature was 850 °C. In addition, time also plays an important role; a longer time (30 min) produces bubbles and inhomogeneous properties, and a shorter time (5 min) gives enameling with better properties (appearance, adhesion, etc.), as Figure 11A showed. This might be due to a lack of time for saturation to occur at the interface.

According to Scrinzi and Rossi [67], degradation of the enamel depends on the thickness and the color. In this case, the applied thickness and the enamel type did not damage the material aesthetically during fire and immersion tests. These tests tried to simulate the service life of the final product. The scratch test showed acceptable enamel adhesion since enamel did not detach with a load of 4 kg.

5. Conclusions

The main aim of this work was enameling and sintering in a single step. To accomplish this, both the iron powder and the enamel were characterized.

Following the powder metallurgy procedure, the compressibility and sinterability of ASC100.29 were studied. As a result, it was found that low sintering temperatures, 835 °C, and low compaction pressures, 500 MPa, were sufficient to obtain enameled parts with high resistance.

The sintering atmosphere of N_2-5H_2 protected the samples during the process by preventing the oxidation of the iron substrate.

Short sintering times, 5 min, also gave better results in enameling since the presence of adhesion agents shortened the firing times and produced a spinel interface favoring chemical anchoring. Furthermore, diffusion is also present since fluxes decrease the temperature, allowing the formation of these spinels. The surface porosity of the substrate also improves the adhesion of enamel by mechanical anchoring.

In summary, the proper parameters to get enameling and sintering samples were 500 MPa of compaction pressure, 850 °C of sintering temperature for 5 min in an N_2-5H_2 atmosphere.

The enamel applied under this condition showed good adhesion with the powder metallurgical steel, representing significant energy saving in the manufacture of gas cooker burners.

Author Contributions: Conceptualization, M.A.M. and J.A.; methodology, M.A.M. and J.A.; validation, M.A.M., J.A. and F.V.; formal analysis, M.A.M., J.A. and F.V.; investigation, M.A.M. and J.A.; resources, M.A.M. and F.V.; data curation, M.A.M. and J.A.; writing—original draft preparation, J.A.; writing—review and editing, M.A.M., J.A., M.B. and F.V.; visualization, J.A.; supervision, M.A.M. and J.A.; project administration, M.A.M.; funding acquisition, M.A.M. and F.V. All authors have read and agreed to the published version of the manuscript. Please turn to the CRediT taxonomy for the term explanation. Authorship must be limited to those who have contributed substantially to the work reported.

Funding: This work has been supported by Comunidad de Madrid (Spain—multiannual agreement with UC3M ("Excelencia para el Profesorado Universitario"-EPUC3M04))—Fifth regional research plan 2016–2020.

Institutional Review Board Statement: Not applicable.

Informed Consent Statement: Not applicable.

Data Availability Statement: Not applicable.

Acknowledgments: Not applicable.

Conflicts of Interest: The authors declare no conflict of interest.

References

1. Ubertazzi, A.; Wojciecjowski, N. *Smalto Porcellanato—Vitreous Enamel*; Ulrico Hoepli Editore: Milano, Italy, 2002.
2. Andrews, A.I. *Porcelain Enamel: The Preparation, Application, and Properties of Enamels*, 2nd ed.; The Garrard Press: Champaign, IL, USA, 1961.
3. Beltrán, M.; Schibille, N.; Brock, F.; Gratuze, B.; Vallcorba, O.; Pradell, T. Modernist enamels: Composition, microstructure and stability. *J. Eur. Ceram. Soc.* **2020**, *40*, 1753–1766. [CrossRef]
4. Rossi, S.; Russo, F. Porcelain Enamel Coating. *Encyclopedia* **2021**, *1*, 388–400.
5. Bodaghi, M.; Davarpanah, A. The influence of cobalt on the microstructure and adherence characteristics of enamel on steel sheet. *Process. Appl. Ceram* **2011**, *5*, 215–222. [CrossRef]

6. Zucchelli, A.; Dignatici, M.; Montorsi, M.; Carlotti, R.; Siligardi, C. Characterization of vitreous enamel–steel interface by using hot stage ESEM and nano-indentation techniques. *J. Eur. Ceram. Soc.* **2012**, *32*, 2243–2251. [CrossRef]
7. Berdzenishvili, I. Functional Corrosion-Resistant Enamel Coatings and Their Adherence Strength. *Acta Phys. Pol.* **2012**, *121*, 178–180. [CrossRef]
8. Pagliuca, S.; Faust, W.D. *Porcelain (Vitreous) Enamels and Industrial Enamelling Processes—The Preparation, Application and Properties of Enamels*; The International Enamellers Institute: Mantua, Italy, 2011.
9. Rossi, S.; Bergamo, L.; Fontanari, V. Fire resistance and mechanical properties of enamelled aluminium foam. *Mater. Des.* **2017**, *132*, 129–137. [CrossRef]
10. Jiang, W.; Wang, Y.; Gu, L. Influence of TiO_2 film on photo-catalytic property of enamels. *J. Noncryst. Solids* **2007**, *353*, 4191–4194. [CrossRef]
11. Chen, L.; Liao, X.; Jiang, W. Effect of heat treatment temperature on super-hydrophilic property of enamels with titanium dioxide thin film. *J. Sol. Gel. Sci. Technol.* **2016**, *80*, 606–611. [CrossRef]
12. Hevia, R.; Centritto, N.; Novaes de Oliveira, P.A.; Bernardín, A.M.; Durán, A. *Introducción a los Esmaltes Cerámicos (Introduction to Ceramic Glazes)*; Durán, A., Ed.; Faenza Editrice Ibérica S.L: Castellón de La Plana, Spain, 2002.
13. Rossi, S.; Parziani, N.; Zanella, C. Abrasion resistance of vitreous enamel coatings in function of frit composition and particles presence. *Wear* **2015**, *332–333*, 702–709. [CrossRef]
14. Zhang, Y.; Zhao, M.; Zhang, J.; Shao, Q.; Li, J.; Li, H.; Lin, B.; Yu, M.; Chen, S.; Guo, Z. Excellent corrosion protection performance of epoxy composite coatings filled with silane functionalized silicon nitride. *J. Polym. Res.* **2018**, *25*, 130. [CrossRef]
15. Longhi, M.; Zini, L.P.; Pistor, V.; Kunst, S.R.; Zattera, A.J. Evaluation of the Mechanic and Electrochemical Properties of an Epoxy Coating with Addition of Different Polyhedral Oligomeric Silsesquioxanes (POSS) Applied on Substrate of Low Alloy Steel. *Mater. Res.* **2017**, *20*, 1388–1401. [CrossRef]
16. Abenojar, J.; Tutor, J.; Ballesteros, Y.; del Real, J.; Martinez, M.A. Erosion-wear, mechanical and thermal properties of silica filled epoxy nanocomposites. *Compos. Part B Eng.* **2017**, *120*, 42–53. [CrossRef]
17. Serenario, M.E.D.; Santos, B.A.F.; de Miranda, L.R.M.; Bueno, A.H.S. Evaluation of the anticorrosive behavior of epoxy-Nb_2O_5 paint in high temperatures submitted to the environment with sulfuric acid. *J. Technol. Res.* **2020**, *17*, 1331–1342. [CrossRef]
18. Pakseresht, A.; Javadi, A.; Bahrami, M.; Khodabakhshi, F.; Simchi, A. Spark plasma sintering of a multilayer thermal barrier coating on Inconel 738 superalloy: Microstructural development and hot corrosion behavior. *Ceram. Int.* **2016**, *42*, 2770–2779. [CrossRef]
19. Lin, B.; Zhong, M.; Zheng, C.; Cao, L.; Wang, D.; Wang, L.; Liang, J.; Cao, B. Preparation and characterization of dopamine-induced biomimetic hydroxyapatite coatings on the AZ31 magnesium alloy. *Surf. Coatings Technol.* **2015**, *281*, 82–88. [CrossRef]
20. Zang, D.; Xun, X. Ceramics Coated Metallic Materials: Methods, Properties and Applications. *Adv. Ceram. Mater.* **2021**. [CrossRef]
21. Hu, W.; Markovych, S.; Tan, K.; Shorinov, O.; Cao, T. Research on Wear Resistance Coating of Aircraft Titanium Alloy Parts by Cold Spraying Technology. *Aerosp. Tech. Technol.* **2020**, *6*, 61–71. [CrossRef]
22. Usana-Ampaipong, T.; Dumkum, C.; Tuchinda, K.; Tangwarodomnukun, V.; Teeraprawatekul, B.; Qi, H. Surface and Subsurface Characteristics of NiCrBSi Coating with Different WC Amount Prepared by Flame Spray Method. *J. Therm. Spray Technol.* **2019**, *28*, 580–590. [CrossRef]
23. Miguel, J.; Guilemany, J.; Vizcaino, S. Tribological study of NiCrBSi coating obtained by different processes. *Tribol. Int.* **2003**, *36*, 181–187. [CrossRef]
24. Bergant, Z.; Trdan, U.; Grum, J. Effect of high-temperature furnace treatment on the microstructure and corrosion behavior of NiCrBSi flame-sprayed coatings. *Corros. Sci.* **2014**, *88*, 372–386. [CrossRef]
25. German, R.M. *Powder Metallurgy and Particulate Materials Processing: The Processes, Materials, Products, Properties, and Applications*; Metal Powder Industries Federation: Princeton, NJ, USA, 2005.
26. Akhtar, S.; Saad, M.; Misbah, M.R.; Sati, M.C. Recent Advancements in Powder Metallurgy: A Review. *Mater. Today Proc.* **2018**, *5*, 18649–18655. [CrossRef]
27. Franco, E.; da Costa, C.E.; Milan, J.C.G.; Tsipas, S.A.; Gordo, E. Multi-component boron and niobium coating on M2 high speed steel processed by powder metallurgy. *Surf. Coatings Technol.* **2020**, *384*, 125306. [CrossRef]
28. Verma, P.; Saha, R.; Chaira, D. Waste steel scrap to nanostructured powder and superior compact through powder metallurgy: Powder generation, processing and characterization. *Powder Technol.* **2018**, *326*, 159–167. [CrossRef]
29. Azevedo, J.M.; CabreraSerrenho, A.; Allwood, J.M. Energy and material efficiency of steel powder metallurgy. *Powder Technol.* **2018**, *328*, 329–336. [CrossRef]
30. Kulkarni, H.; Dabhade, V.V. Green machining of powder-metallurgy-steels (PMS): An overview. *J. Manuf. Process.* **2019**, *44*, 1–18. [CrossRef]
31. Abdallah, A.; Habibnejad-Korayem, M.; Malakhov, D.V. Are Large Particles of Iron Detrimental to Properties of Powder Metallurgy Steels? *Metals* **2020**, *10*, 431. [CrossRef]
32. Pérez-Velásquez, S.; Pineda-Triana, Y.; Vera-López, E.; Sarmiento-Santos, A. Influence of compaction pressure in steel composites AISI 316 reinforced with titanium carbide against wear. *Ing. Comp.* **2016**, *18*, 163–174.
33. Abenojar, J.; Velasco, F.J.; Bautista, M.A.; Campos, M.; Bas, J.; Torralba, J.M. Atmosphere influence in sintering process of stainless steels matrix composites reinforced with hard particles. *Compos. Sci. Technol.* **2003**, *63*, 69–79. [CrossRef]

34. Oke, S.R.; Ige, O.O.; Falodun, O.E.; Okoro, A.M.; Mphahlele, M.R.; Olubambi, P.A. Powder metallurgy of stainless steels and composites: A review of mechanical alloying and spark plasma sintering. *Int. J. Adv. Manuf. Technol.* **2019**, *102*, 3271–3290. [CrossRef]
35. Abenojar, J.; Bautista, A.; Guzmán, S.; Velasco, F.J.; Martinez, M.A.; Bautista, M.A. Microstructural influence on corrosion properties of aluminium composites reinforced with amorphous iron borides. *Mater. Corros.* **2012**, *65*, 678–684. [CrossRef]
36. Chamroune, N.; Mereib, D.; Delange, F.; Caillault, N.; Lu, Y.; Grosseau-Poussard, J.-L.; Silvain, J.-F. Effect of flake powder metallurgy on thermal conductivity of graphite flakes reinforced aluminum matrix composites. *J. Mater. Sci.* **2018**, *53*, 8180–8192. [CrossRef]
37. Deng, Z.; Yin, H.; Zhang, C.; Zhang, G.; Li, W.; Zhang, R.; Jiang, X.; Qu, X. Microstructure and mechanical properties of Cu–12Al–xNi alloy prepared using powder metallurgy. *Mater. Sci. Eng. A* **2019**, *759*, 241–251. [CrossRef]
38. Li, J.; Hu, R.; Yang, J.; Gao, Z.; Zhang, K.; Wang, X. Evolution and micromechanical properties of interface structures in TiNbf/TiAl composites prepared by powder metallurgy. *J. Mater. Sci.* **2020**, *55*, 12421–12433. [CrossRef]
39. Wang, H.; Fang, Z.Z.; Sun, P. A critical review of mechanical properties of powder metallurgy Titanium. *Inter J. Powder Met.* **2010**, *46*, 45–57.
40. Fang, Z.Z.; Paramore, J.D.; Sun, P.; Chandran, K.S.R.; Zhang, Y.; Xia, Y.; Cao, F.; Koopman, M.; Free, M. Powder metallurgy of titanium—past, present, and future. *Int. Mater. Rev.* **2018**, *63*, 407–459. [CrossRef]
41. Fer, B.; Tingaud, D.; Hocini, A.; Hao, Y.; Leroy, E.; Prima, F.; Dirras, G. Powder Metallurgy Processing and Mechanical Properties of Controlled Ti-24Nb-4Zr-8Sn Heterogeneous Microstructures. *Metals* **2020**, *10*, 1626. [CrossRef]
42. Miryala, M.; Arvapalli, S.S.; Diko, P.; Jirsa, M.; Murakami, M. Flux Pinning and Superconducting Properties of Bulk MgB_2 with MgB_4 Addition. *Adv. Eng. Mater.* **2019**, *22*, 1900750. [CrossRef]
43. Tuminoh, H.; Hermawan, H.; Ramlee, M. Optimum Processing of Absorbable Carbon Nanofiber Reinforced Mg–Zn Composites Based on Two-Level Factorial Design. *Metals* **2021**, *11*, 278. [CrossRef]
44. Dos Santos, D.T.; Salemi, A.; Cristofolini, I.; Molinari, A. The tensile properties of a Powder Metallurgy Cu–Mo–Ni diffusion bonded steel sintered at different temperatures. *Mater. Sci. Eng. A* **2019**, *759*, 715–724. [CrossRef]
45. Parvizi, S.; Hashemi, S.M.; Asgarinia, F.; Nematollahi, M.; Elahinia, M. Effective parameters on the final properties of NiTi-based alloys manufactured by powder metallurgy methods: A review. *Prog. Mater. Sci.* **2021**, *117*, 100739. [CrossRef]
46. Abenojar, J.; Velasco, F.J.; Mota, J.; Martinez, M. Preparation of Fe/B powders by mechanical alloying. *J. Solid State Chem.* **2004**, *177*, 382–388. [CrossRef]
47. Dehghan-Manshadi, A.; Kent, D.; St John, D.; Dargusch, M. Properties of Powder Metallurgy-Fabricated Oxygen-Containing Beta Ti–Nb–Mo–Sn–Fe Alloys for Biomedical Applications. *Adv. Eng. Mater.* **2020**, *22*, 1901229. [CrossRef]
48. Bolzoni, L.; Yang, F. Development of Cu-bearing powder metallurgy Ti alloys for biomedical applications. *J. Mech. Behav. Biomed. Mater.* **2019**, *97*, 41–48. [CrossRef] [PubMed]
49. Dewidar, M.M.; Yoon, H.-C.; Lim, J.K. Mechanical properties of metals for biomedical applications using powder metallurgy process: A review. *Met. Mater. Int.* **2006**, *12*, 193–206. [CrossRef]
50. Staf, H.; Kis, Z.; Szentmiklósi, L.; Kaplan, B.; Olsson, E.; Larsson, P.-L. Determining the density distribution in cemented carbide powder compacts using 3D neutron imaging. *Powder Technol.* **2019**, *354*, 584–590. [CrossRef]
51. Gaille, B. 18 Powder Metallurgy Industry Statistics and Trends. 17 October 2018. Available online: https://brandongaille.com/18-powder-metallurgy-industry-statistics-and-trends/ (accessed on 29 November 2020).
52. Manohar, G.; Dey, A.; Pandey, K.M.; Maity, S.R. Fabrication of metal matrix composites by powder metallurgy: A review. In Proceedings of the AIP Conference Proceedings, Gaithersburg, MD, USA, 24 April 2018; AIP Publishing: College Park, MD, USA, 2018; Volume 1952, p. 020041. [CrossRef]
53. Zhang, M.; Wang, X.; Dupuy, A.; Schoenung, J.; Li, X. Study on Strain Rate–Dependent Deformation Mechanism of WC–10 wt% Ni_3 Al Cemented Carbide by Micropillar Compression. *Adv. Eng. Mater.* **2019**, *22*, 1900953. [CrossRef]
54. Ahmed, M.M.Z.; Barakat, W.S.; Mohamed, A.Y.A.; Alsaleh, N.A.; Elkady, O.A. The Development of WC-Based Composite Tools for Friction Stir Welding of High-Softening-Temperature Materials. *Metals* **2021**, *11*, 285. [CrossRef]
55. Song, D.; Tang, R.; Yang, F.; Qiao, Y.; Sun, J.; Jiang, J.; Ma, A. Development of High-Performance Enamel Coating on Grey Iron by Low-Temperature Sintering. *Materials* **2018**, *11*, 2183. [CrossRef]
56. Höganäs. *Production of Sintered Components in Höganäs Handbood for Sintered Components*; Höganäs: Luleå, Sweden, 1997; Volume 2.
57. CEN. *EN 10209. Cold Rolled Low Carbon Steel Flat Products for Vitreous Enamelling—Technical Delivery Conditions*; CEN: Brussels, Belgium, 2013.
58. CEN. *EN 10025-2. Hot Rolled Products of Structural Steels—Part 2: Technical Delivery Conditions for non-Alloy Structural Steels*; CEN: Brussels, Belgium, 2020.
59. CEN. *EN 10111. Continuously Hot Rolled Low Carbon Steel Sheet and Strip for Cold Forming—Technical Delivery Conditions*; CEN: Brussels, Belgium, 2009.
60. Household Cooking Appliance Market Size, Share & Trends Analysis Report by Product (Cooktops & Cooking Ranges, Ovens, Specialized Appliances), By Region, And Segment Forecasts, 2019–2025 in: Market Analysis Report. 2019. Available online: https://www.grandviewresearch.com/industry-analysis/household-cooking-appliances-market (accessed on 25 January 2021).
61. Todo Para mi Hogar. Available online: https://www.todoparamihogar.com/Burner-cap-Teka (accessed on 2 January 2021).
62. Höganäs. *Material and Powder Properties in Höganäs Handbood for Sintered Components*; Höganäs: Luleå, Sweden, 1997; Volume 1.

63. Technical Sheet ASC 100.29 Höganäs. 2016. Available online: https://www.hoganas.com/en/powder-technologies/pressing-sintering/products/iron-powders/ (accessed on 2 February 2021).
64. Porcelain Enamel Powders. Available online: https://www.ferro.com/products/product-category/porcelain-enamel-coatings/porcelain-enamel-coatings/porcelain-enamel-powders/porcelain-enamel-powders (accessed on 2 February 2021).
65. Aksel, C. Spinel Formation, Reaction Conditions and Densification Properties of Magnesia-Spinel Composites. *Key Eng. Mater.* **2004**, *264*, 1071–1074. [CrossRef]
66. Van Everbroeck, T.; Ciocarlan, R.-G.; Van Hoey, W.; Mertens, M.; Cool, P. Copper-Containing Mixed Metal Oxides (Al, Fe, Mn) for Application in Three-Way Catalysis. *Catalysts* **2020**, *10*, 1344. [CrossRef]
67. Scrinzi, E.; Rossi, S. The aesthetic and functional properties of enamel coatings on steel. *Mater. Des.* **2010**, *31*, 4138–4146. [CrossRef]